Atomistic Modeling of a New Thermoplastic Polyimide in the Amorphous State: Structure and Energetics

Renshi Zhang and Wayne L. Mattice*

The Maurice Morton Institute of Polymer Science, The University of Akron, Akron, Ohio 44325-3909

Received December 19, 1994; Revised Manuscript Received February 27, 1995[⊗]

ABSTRACT: Atom-based molecular modeling is conducted for the study of the bulk properties of a recently developed semicrystalline polyimide of 3,3′,4,4′-benzophenonetetracarboxylic dianhydride (BTDA) and 2,2-dimethyl-1,3-(4-aminophenoxy)propane (DMDA) in the amorphous phase at the experimental density of room temperature. This polyimide is abbreviated as PI-2. A short-time high-temperature molecular dynamics procedure is performed in order to relax the PI-2 structures. The energy of each structure is subsequently minimized using molecular mechanics to form the final structures for our study. Ten different amorphous structures were constructed in order to determine the precision of our study by inspecting the standard deviations. Electrostatic interactions are explicitly considered by assignment of proper partial charges to individual atoms, and the Ewald summation method is employed for evaluation of the nonbonded interactions. The radial distribution functions of the atoms appear to show no long-range order, assuring the amorphous nature of the built structures. The correlation between the phenyl rings in the systems suggests that there is local order in the range of 3−4.5 Å between the rigid ring units due to the van der Waals interactions. The conformational statistics of the polymer backbone in the amorphous structure are compared with those of a PI-2 single chain in vacuum at 300 K, obtained from an earlier study. The differences indicate the effect of packing at bulk density. The calculation of the dimensionless characteristic ratio of the end-to-end distance suggests that the PI-2 chain in the bulk amorphous phase is less extended than a PI-2 single chain in vacuum at 300 K. For a single chain in vacuum, $C_\infty = 6.4$, while for the bulk structures, $C_\infty = 5.0$. This reduction in C_∞ arises almost entirely from the appearance of two new rotational isomeric states at a pair of equivalent bonds in the repeat unit. The Hildebrand solubility parameter of amorphous PI-2 calculated from the cohesive energy density yields a value of ~11.3 $(cal/cm^3)^{1/2}$.

Introduction

A necessary and natural advantage of atom-based molecular modeling is that it can reveal the mechanisms of physical processes on microscopic scales, which sometimes proves to be difficult from experimental studies. The macroscopic properties, many of which can be measured by experiments, can also be obtained from molecular modeling by equilibrium or time-dependent statistics. Currently, fully atomistic modeling is restricted in the time scale and the size of the systems that one can model because of the limitations of the computer power. However, even with these limitations, there have been successes in the studies of a wide variety of polymer properties through atomistic modeling. For example, researchers have studied the chain dynamics near the glass transition temperature,[1] the cohesive energy density and Hildebrand solubility parameter in bulk amorphous polymers,[2−6] the bond orientation correlation functions and atomic radial distribution functions,[2−9] the free volume distributions in the bulk amorphous phase,[10−13] and the diffusion of small molecules in a polymer matrix.[14−18] Most of the attempts have been made on structurally simple polymer systems such as polyethylene,[1,7,10,14,15,19−21] polypropylene,[2,16] poly(vinyl chloride),[4,9,22] and polybutadiene,[5,6,13] with a few recent studies focusing on structurally more complex polymers, such as polycarbonate[3,17,18,23−25] and polysulfone.[8]

In this paper, we report the study of the amorphous state of a new thermoplastic semicrystalline polyimide, synthesized from 3,3′,4,4′-benzophenonetetracarboxylic dianhydride (BTDA) and 2,2-dimethyl-1,3-(4-aminophenoxy)propane (DMDA),[26] using atomistic modeling. The molecular weight and atomic composition of the repeat unit are 572 and $C_{34}H_{24}O_7N_2$, respectively. This polyimide, with the compact name of PI-2, has a glass transition temperature T_g of 230 °C and a melting point T_m of 325 °C.[27] This narrow "crystallization window" gives PI-2 a relatively high usage temperature for its processing temperature and makes it a good candidate as a matrix material in the high-temperature, high-performance polymer composites. Other good properties of PI-2 include thermooxidative stability, solvent resistance, and excellent mechanical properties.[26,27] The highest degree of crystallinity of PI-2 achieved to date is 50%.[27] The understanding of the amorphous phase of PI-2 is therefore of importance to the role that PI-2 plays in a polymer composite. In this work we use atomistic modeling to study the bulk properties of amorphous PI-2, including the atomic radial distribution functions, the conformational statistics through the dihedral angle distributions, the correlations between the phenyl rings in the systems, the characteristic ratio of PI-2 in the amorphous bulk, and the cohesive energy density and Hildebrand solubility parameter. Comparisons are made between the dihedral angle distributions of a PI-2 chain in the bulk and a PI-2 single chain in vacuum at 300 K.[28] Similar comparisons are made for the characteristic ratios as well. The effect of packing the chains in a bulk structure is seen through these comparisons.

Method

PI-2 is to date structurally the most complex polymer among the ones that have been studied with atomistic modeling in the amorphous state at bulk density. The repeat unit of PI-2, as shown in Figure 1, consists of 67 atoms. Four virtual bonds (1, 4, 5, and 10 in Figure 1) and six covalent bonds (2, 3, 6, 7, 8, and 9 in Figure 1)

[⊗] Abstract published in *Advance ACS Abstracts,* April 15, 1995.

0024-9297/95/2228-7454$09.00/0

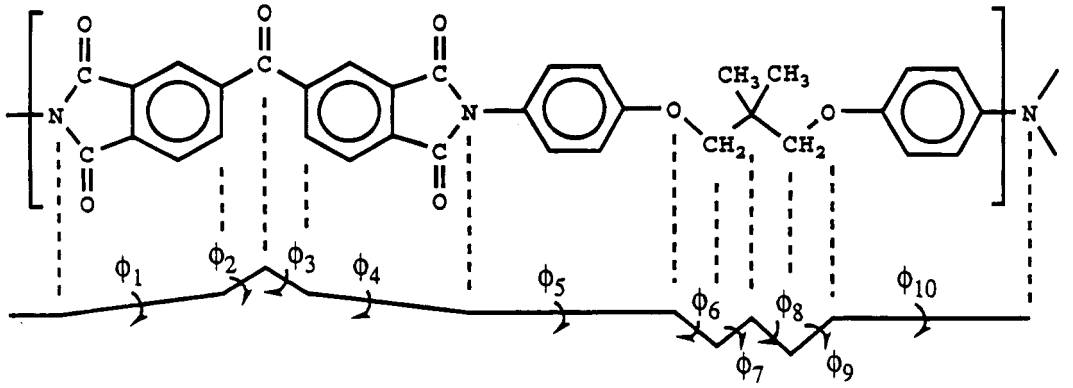

Figure 1. Repeat unit and the virtual bonds of PI-2. Hydrogen atoms on the rings are now shown, but they are included in the calculation. ϕ_i is the torsion about bond, or virtual bond, i.

are used to trace the chain through the large repeat unit. To study the bulk properties of amorphous PI-2, we first need to build the amorphous structures. Two methods are established for building an amorphous structure of a polymer.[1,2] One method, proposed by Theodorou and Suter, starts by creating an initial guess structure by packing a "parent" chain into a unit cell at the specified bulk density and then minimizes the energy of the structure.[2] The other method, proposed by Rigby and Roe, creates representative initial configurations by placing all constituent atoms in an atomic liquid configuration and then slowly turns on all bonded interactions of the polymer during a subsequent molecular dynamics run for a relaxation of the structure.[1] Periodic boundary conditions are applied in both methods for simulation of interchain interactions in the bulk. As the constituency of the system becomes more complex, the second method becomes less efficient. In this study, we choose a molecular modeling software package, POLYGRAF, which uses the approach of the first method.

The DREIDING II force field[29] was used for the energy calculations. The potential energy takes contributions from the following terms:

$$E = E_l + E_\theta + E_\phi + E_{inv} + E_{vdW} + E_{Coul} \quad (1)$$

where E_l, E_θ, and E_ϕ are the bond stretching, bond angle bending, and torsion terms, E_{inv} is the improper out-of-plane interaction of a cyclic group, and E_{vdW} and E_{Coul} are the nonbonded van der Waals and Coulomb interactions. A dielectric constant of 3.4, appropriate for polyimides, was chosen for the calculation of the Coulomb interactions.[30] The Ewald summation method is used for evaluating the nonbonded interactions.

The building of the PI-2 structures is as follows: (1) A monomer of PI-2 is created. (2) All atoms in the monomer are assigned with partial charges computed with the charge-equilibrium method of Rappé and Goddard.[31] (3) A parent chain of PI-2 is created from the monomer, with a degree of polymerization x (x = 13 or 14). (4) An amorphous unit cell of PI-2 is created by packing the PI-2 chain into a cubic box with an edge length of 21.1 Å (for x = 13) or 21.7 Å (for x = 14), so that the density of the amorphous cell will correspond to the experimental density, 1.307 g/cm^3, of PI-2. The sides of the periodic box are nearly twice as large as the calculated persistence length (12.7 Å) for the isolated chain.[28] We create a total of five unit cells with x = 13 and five unit cells with x = 14.

The internal stress of the initial structures usually cannot be reduced sufficiently by a simple energy minimization. Steric hindrances caused by the building process tend to force the initial structures into local energy minima which usually have rather high energy values. For the structures to be well relaxed, we perform molecular dynamics at a temperature of 1000 K for 4 ps after the initial energy minimization. The use of a very high temperature is intended for creating enough conformational motions so that the structures can move out of the local energy minima in a relatively short period of time. The molecular dynamics is performed under constant volume constraint in order to keep the density of the systems unchanged during the high-temperature relaxation process. The time step used for this process is 1 fs. A snapshot is taken at every time step during the trajectory. Among these snapshots, we choose the conformer with the lowest energy and then perform an energy minimization of this conformer. By this time we have obtained a final structure.

Results and Discussion

1. Radial Distribution Functions. The intermolecular radial distribution functions between a specific pair of atom types in a structure reveal the correlations between the specific atom types in the structure. The average radial distribution functions over all atom types can be used to judge if the system is truly amorphous. The radial distribution function, $g_{AB}(r)$, between a pair of atoms of type A and type B separated by a distance r, is defined by

$$dN_{AB}(r) = \varrho_{AB}(r)\, g_{AB}(r)\, d^3r \quad (2)$$

where ϱ_{AB} is the density of atom pairs of type AB and $dN_{AB}(r)$ is the number of AB pairs separated by a distance in the range $r \sim r + dr$. The radial distribution functions between specific atom pairs do not reveal apparent order at short range or long range. Here we show the radial distribution function averaged over all atom pairs in the systems in Figure 2. The interchain radial distribution function, shown in the inset of Figure 2, indeed reveals no apparent order. Such a finding provides assurance that the structures we obtained from the earlier processes are indeed amorphous.

2. Correlation between Orientations of the Phenyl Rings. It is of interest to study any correlations that might exist between substructures even though the overall structure shows no long-range order. As an example, we study the correlation between the orientations of the phenyl rings in the amorphous PI-2 structures.

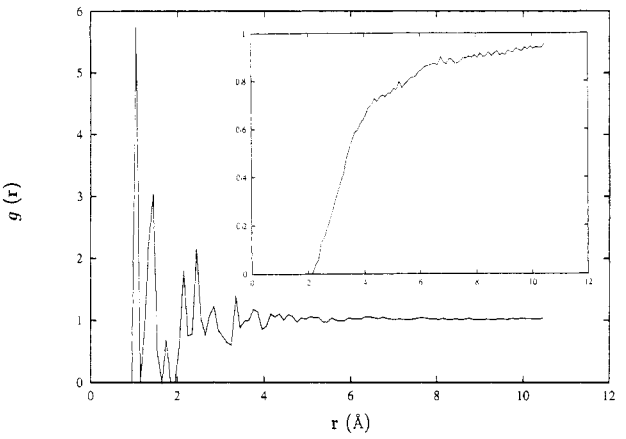

Figure 2. Atomic radial distribution function averaged over all atom pairs. Inset: interchain atomic radial distribution function.

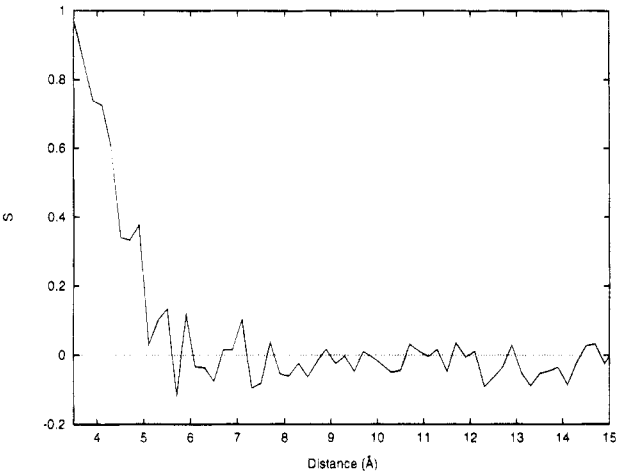

Figure 3. Correlation between the normals of two phenyl rings as a function of their separation.

The orientation of a phenyl ring can be defined by its normal. Because of the symmetry associated with a 180° flip of the phenyl ring, it is best to describe this correlation by the average second-order Legendre polynomial

$$S = \frac{1}{2}(3\langle\cos^2\theta\rangle - 1) \qquad (3)$$

where θ is the angle between the normals of any two phenyl rings under consideration. For a random distribution of phenyl rings, cos θ is random, which leads to $S = 0$. For a perfectly correlated case, in which all phenyl rings are parallel, cos $\theta \equiv 1$ and $S = 1$. Geometrically nearby planar ring structures might favor some alignment so that the interchain repulsive energy might be reduced. It is desirable to study over how long a distance this kind of alignment persists. In Figure 3 we plot S as a function of the separation between two phenyl rings while considering all phenyl ring pairs. The separation is defined by the distance between the centers of the phenyl rings. We plot the result for the range 3.5−15 Å since all phenyl rings in the systems are separated by at least 3.5 Å and the number of statistical samples becomes small beyond 15 Å. From this figure it can be clearly seen that, beyond 5 Å, there is no correlation between, or alignment of, the phenyl rings. Between 3.5 and 5 Å, the normals of the phenyl rings tend to be parallel to each other. A similar phenomenon has been found in a study of amorphous

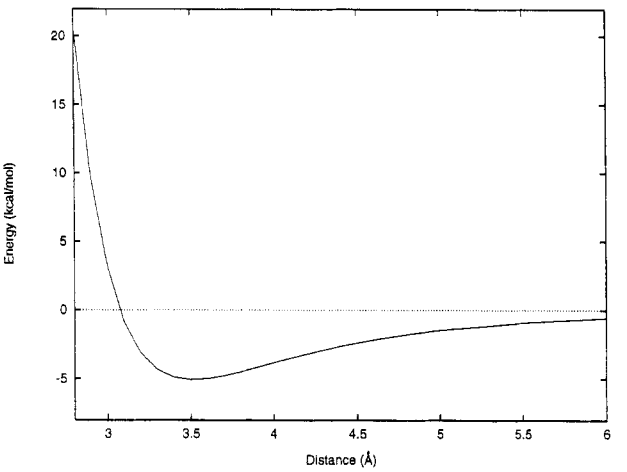

Figure 4. Intermolecular potential energy between two benzene molecules as a function of separation with the configuration described in the text.

polystyrene.[32] In order to understand this behavior, we made a study of a model system with two benzene molecules only. The lowest energy and the nearest distance between the two benzene molecules can be achieved by having the molecular planes parallel to each other and perpendicular to the axis connecting the ring centers, while having the hydrogen atoms on both molecules remain in a staggered configuration. The intermolecular potential energy between the two benzene molecules is plotted in Figure 4 as a function of the separation. It can be seen that the minimum energy is reached at 3.5 Å. Other configurations between the orientations of the benzene rings all lead to higher energies, which explains why there is positive correlation at short distances between the orientations of the phenyl rings in PI-2. At larger distances the effect of van der Waals interactions becomes very small, and any correlation between the phenyl rings is diminished.

Therefore, we reach the conclusion that, at short distances, neighboring rings tends to remain parallel to each other due to van der Waals interactions. However, such order completely disappears as the distance is increased to as little as 5 Å. The ring orientation follows a random distribution for distances beyond 5 Å, which proves again that no long-range order exists in the system.

3. Dihedral Angle Distributions. The conformational behavior of a polymer chain can be described by the dihedral angle distributions. Comparison of the dihedral angle distributions of a polymer chain in the bulk and a single chain in vacuum can give indications to the effect of chain packing. For the purpose of comparison, we use the results from a molecular dynamics study of a PI-2 single chain in vacuum at 300 K.[28] In that study, a great number of conformational transitions were observed at certain virtual bonds along the backbone during the 2.2 ns molecular dynamics trajectory. The distribution of such dihedral angles in time therefore is a reliable statistic because of the large sampling size. In a bulk structure, conformational transitions occur only at a much slower rate. It is therefore not an efficient way to study the dihedral angle distributions by molecular dynamics because of the tremendous amount of CPU time required. The difficulty can be circumvented by building a number of amorphous cells and studying the static dihedral angle distributions of this ensemble. We have in the 10 amorphous cells a total of 270 bonds of each type, which provide a reasonable sampling size.

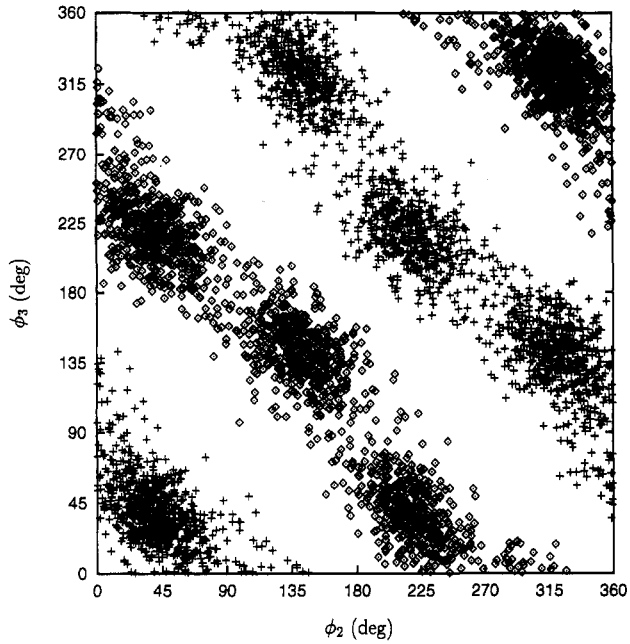

Figure 5. Distribution of (ϕ_2,ϕ_3) in the 2.2 ns single-chain molecular dynamics trajectory at 300 K. The points plotted as diamonds were observed directly in the trajectory; the points plotted as crosses are the mirror images.

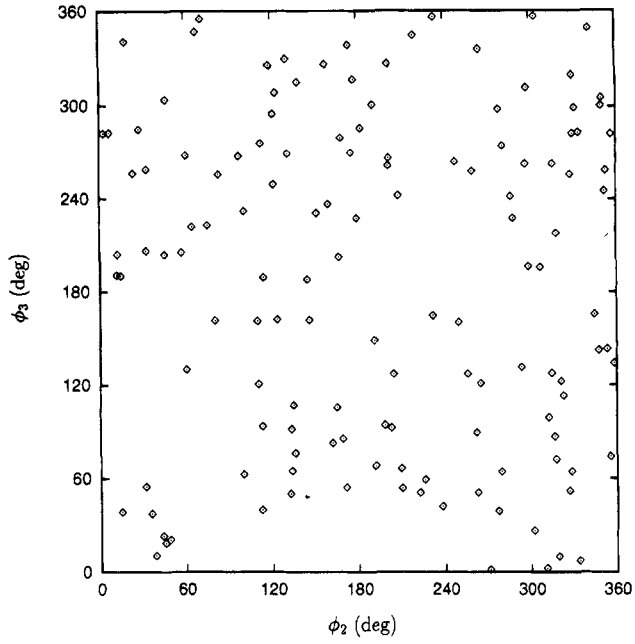

Figure 6. Distribution of (ϕ_2,ϕ_3) in the ensemble of 10 amorphous cells.

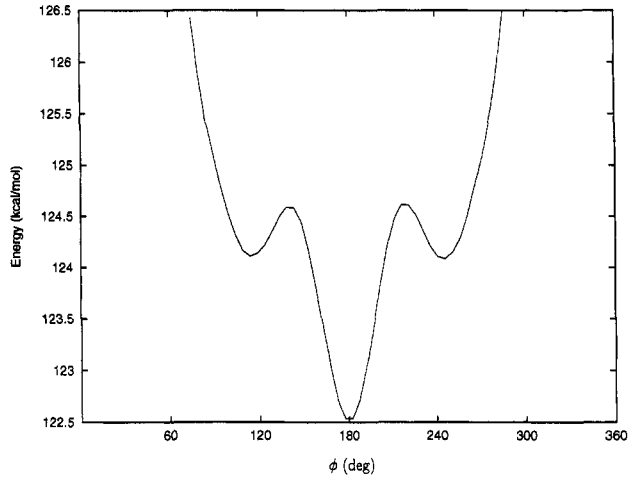

Figure 7. Potential energy curve of ϕ_6.

The biggest differences between the dihedral angle distributions in the amorphous cells and in the single chain seem to lie in the equivalent bonds 2 and 3 and the equivalent bonds 6 and 9 (bonds are defined in Figure 1). In the single-chain dynamics trajectory,[28] many cooperative conformational changes have been observed at bonds 2 and 3. In Figure 5 we plot the distribution of (ϕ_2,ϕ_3) for the single-chain trajectory. Considerations of the symmetry of the torsion potential energy function at bonds 2 and 3, and also the joint conformational energy surface for these two bonds, show that there are two nearly continuous bands of low energy that correspond approximately to the equations $\phi_3 = -90° - \phi_2$ and $\phi_3 = 90° - \phi_2$. The barrier height for transitions between these two bands is high enough so that no such transition was observed during the trajectory for the isolated chain. Therefore, the observations in the trajectory (diamonds; Figure 5) only provide information about the low-energy band that approximates $\phi_3 = -90° - \phi_2$. In order to represent the energetically equivalent band with $\phi_3 = 90° - \phi_2$, we include crosses in Figure 5, which are the mirror images of the conformations denoted by diamonds. Considering the diamonds and crosses together, it is evident that certain regions of (ϕ_2,ϕ_3) are preferred over others in the isolated chain.

In the ensemble of the 10 amorphous cells, it seems that (ϕ_2,ϕ_3) are distributed almost randomly, as shown in Figure 6, even though such a distribution would cause higher intrachain potentials. The rigidity of the segments spanned by virtual bonds 3, 4, and 5 (and equivalently by virtual bonds 2, 1, and 10) makes it difficult to lower simultaneously the intrachain energy and the interchain energy in the amorphous structures. The reduction of the interchain energy by an effective packing of the chain segments in this case apparently compensates the expense of an increase in the intrachain energy.

A grid search of the energy of rotation about bond 6 produces the curve in Figure 7. The potential energy outside the plotted range is more than 4 kcal/mol higher than the energy at $\phi_6 = 180°$. In the single-chain molecular dynamics trajectory, the distribution of ϕ_6 and ϕ_9 has three peaks (Figure 8), corresponding to the three energy minima in Figure 7. In the ensemble of the 10 amorphous cells this distribution exhibits two additional peaks near 75° and 285° (Figure 8). These additional peaks are close to the locations of *gauche* and *gauche'* for the neighboring bonds 7 and 8 (Figure 9). These new peaks again might be an indication of the difficulty in packing a chain with some rigid segments in the structure. As was noted previously, bonds 0 (equivalent of bond 10) through 5 are rather rigid. In order to achieve an effective packing, bonds 6 and 9 have to be rotated in order to produce a local structure that will lower the energy. Such a rotation is facilitated by adopting conformations close to the *gauche* and *gauche'* states so that some of the conformations near the segment from bonds 5 through 10 could resemble the flexibilities of simple olefins, which will lower the interchain energy. In other words, through a concerted rotation of bonds 6 through 9, it is relatively easy to achieve a low intrachain energy without significantly increasing the interchain energy. The distribution of the dihedral angles at bonds 7 and 8 in the amorphous

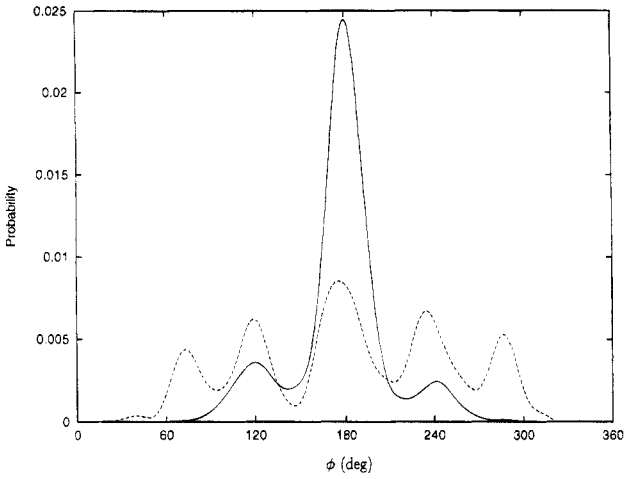

Figure 8. Probability distributions of ϕ_6 and ϕ_9 in the single-chain molecular dynamics at 300 K (solid line) and in the amorphous cells (dashed line).

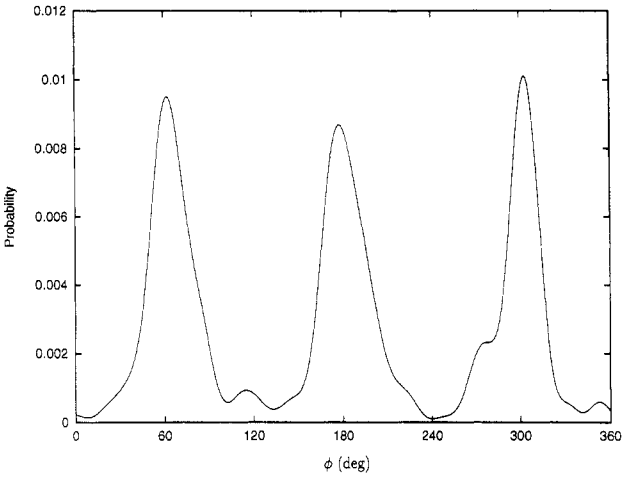

Figure 9. Probability distribution of ϕ_7 and ϕ_8 in the amorphous cells.

cells (Figure 9), on the other hand, almost reproduces the result of the single chain.[28]

4. Characteristic Ratio. The effect of interchain interaction on chain conformations in the bulk can also be reflected by a change in the limiting characteristic ratio, which is defined as the limit of C_n as $n \to \infty$[33]

$$C_n \equiv \langle r^2 \rangle / \sum_{i=1}^{n} l_i^2 \tag{4}$$

Here $\langle r^2 \rangle$ is the mean-square end-to-end distance of the chain, n is the number of bonds and virtual bonds along the backbone, and l_i are the lengths of these bonds and virtual bonds. A simple way to calculate the characteristic ratio, given a large number of chains, is by a direct measurement of the squared end-to-end distances and division of the average by $\sum_{i=1}^{n} l^2$, which is also obtained by measurement. When the sample of chains is small, as in our case, such a simple treatment could lead to a sizable statistical error. A better way to calculate the characteristic ratio is through the transformation matrix method,[28,34] which uses statistical averages of the bond lengths, bond angles, and dihedral angles as input of the transformation matrices and arrives at a statistical result. Although there are only 10 parent chains in our systems, the total number of bonds of each type is ~270. Therefore, the result from the transformation matrix method should undoubtedly be more reliable than the simple treatment mentioned above. Since the interdependency between the virtual bonds does not significantly affect the value of the characteristic ratio for this chain when it is isolated,[28] we will use the independent bond model for our calculation.

The transformation matrix has the form[35]

$$\mathbf{T}_i = \begin{pmatrix} -\cos\theta_i & \sin\theta_i & 0 \\ -\sin\theta_i \cos\phi_i & -\cos\theta_i \cos\phi_i & -\sin\phi_i \\ -\sin\theta_i \sin\phi_i & -\cos\theta_i \sin\phi_i & \cos\phi_i \end{pmatrix} \tag{5}$$

where θ_i is the angle between bonds $i+1$ and i, and ϕ_i is the dihedral angle at bond i, with $\phi = 180°$ defined as *trans*. The transformation matrices lead to the formation of the generator matrices, $\mathbf{G}_i$, which are used to evaluate the mean-square end-to-end distance of the chains, viz.[35]

$$\langle r^2 \rangle = \langle \mathbf{G}_1 \mathbf{G}_2 ... \mathbf{G}_{n-1} \mathbf{G}_n \rangle \tag{6}$$

where

$$\mathbf{G}_1 = (1 \quad 2\mathbf{l}_1^{\mathrm{T}} \mathbf{T}_1 \quad \mathbf{l}_1^2) \tag{7}$$

$$\mathbf{G}_i = \begin{pmatrix} 1 & 2\mathbf{l}_i^T \boldsymbol{T}_i & \mathbf{l}_i^2 \\ \mathbf{0} & \mathbf{T}_i & \mathbf{l}_i \\ 0 & \mathbf{0} & 1 \end{pmatrix} \qquad 1 < i < n \tag{8}$$

and

$$\mathbf{G}_n = \begin{pmatrix} \mathbf{l}_n^2 \\ \mathbf{l}_n \\ 1 \end{pmatrix} \tag{9}$$

In the above equations, $\mathbf{l}_i$ are the bond or virtual bond vectors, defined as

$$\mathbf{l}_i = \begin{pmatrix} l_i \\ 0 \\ 0 \end{pmatrix} \tag{10}$$

and $\mathbf{l}_i^{\mathrm{T}}$ is the transpose of $\mathbf{l}_i$.

For a polymer chain with independent virtual bonds, the average product of the generator matrices in eq 6 is equal to the product of the average generator matrices, i.e.

$$\langle r^2 \rangle = \langle \mathbf{G}_1 \rangle \langle \mathbf{G}_2 \rangle ... \langle \mathbf{G}_{n-1} \rangle \langle \mathbf{G}_n \rangle \tag{11}$$

and $\langle \mathbf{G}_i \rangle$ can be calculated with knowledge of $\langle \mathbf{T}_i \rangle$. Since the bond lengths fluctuate in a small range at very high frequencies, we can treat them as constants with their average values. The only task then is to calculate the average angular properties of the individual bonds.

Some of the average angular functions can be conveniently assigned with zero values according to the symmetry of the polymer chain. For example, the symmetry of the torsion potential energy function requires $\langle \sin\phi_i \rangle = 0$ for all bonds which, along with the assumption of the independence of θ_i and ϕ_i, simplifies the average transformation matrices to

$$\langle \mathbf{T}_i \rangle = \begin{pmatrix} -\langle \cos\theta_i \rangle & \langle \sin\theta_i \rangle & 0 \\ -\langle \sin\theta_i \rangle \langle \cos\phi_i \rangle & -\langle \cos\theta_i \rangle \langle \cos\phi_i \rangle & 0 \\ 0 & 0 & \langle \cos\phi_i \rangle \end{pmatrix} \tag{12}$$

The symmetry in the potential energy contour map of ϕ_2 and ϕ_3 makes $\langle \cos\phi_2 \rangle = \langle \cos\phi_3 \rangle = 0$.[28] For bonds 5

Table 1. Average Lengths of the Virtual Bonds (Å)

i	1, 4	2, 3	5, 10	6, 9	7, 8
$\langle l_i \rangle_{bulk}$	4.62	1.41	5.53	1.44	1.57
$\langle l_i \rangle_{single\ chain}$	4.62	1.41	5.56	1.44	1.57

Table 2. Average Sines and Cosines of the Angles between Virtual Bonds i and $i + 1$

i	1, 3	2	4, 10	5, 9	6, 8	7
$\langle \cos \theta_i \rangle_{bulk}$	−0.922	−0.561	−0.949	−0.630	−0.397	−0.346
$\langle \cos \theta_i \rangle_{single\ chain}$	−0.930	−0.561	−0.981	−0.673	−0.376	−0.334
$\langle \sin \theta_i \rangle_{bulk}$	0.382	0.826	0.280	0.767	0.917	0.938
$\langle \sin \theta_i \rangle_{single\ chain}$	0.364	0.827	0.184	0.737	0.925	0.941

Table 3. Average Cosines of the Dihedral Angles at Virtual Bond i

i	1, 4	2, 3	5, 10	6, 9	7, 8
$\langle \cos \phi_i \rangle_{bulk}$	0.629	0.000	0.000	−0.427	0.000
$\langle \cos \phi_i \rangle_{single\ chain}$	0.837	0.000	0.000	−0.867	0.000

and 10, the symmetry of the phenyl rings makes $\langle \cos \phi_5 \rangle = \langle \cos \phi_{10} \rangle = 0$. For bonds 7 and 8, the rotational potentials are nearly 3-fold symmetric because of the presence of the dimethyl groups. Therefore, $\langle \cos \phi_7 \rangle = \langle \cos \phi_8 \rangle = 0$. The transformation matrices for these bonds are thus simplified further to

$$\langle \mathbf{T}_i \rangle = \begin{pmatrix} -\langle \cos \theta_i \rangle & \langle \sin \theta_i \rangle & 0 \\ 0 & 0 & 0 \\ 0 & 0 & 0 \end{pmatrix} \tag{13}$$

The rest of the averages in eq 12 and the average bond lengths need to be evaluated from the molecular dynamics trajectory in the case of a single chain or from the ensemble of amorphous cells, which is the current case. The average bond lengths are listed in Table 1, the average sine and cosine of the bond angles are listed in Table 2, and the average cosine of the dihedral angles are listed in Table 3.

The characteristic ratio can be calculated according to eqs 4−13. For convenience, we introduce the concept of an effective generator matrix, which is the product of 10 consecutive generator matrices in a repeat unit. For example, if we start from the first bond in Figure 1, the effective 5 × 5 generator matrix will be

$$\mathbf{G} = \langle \mathbf{G}_1 \rangle \langle \mathbf{G}_2 \rangle ... \langle \mathbf{G}_{10} \rangle \tag{14}$$

using the 5 × 5 representation, eq 8, for $\langle \mathbf{G}_1 \rangle$. This way the characteristic ratio can be calculated as a function of the number of repeat units, N, instead of the number of individual bonds, n, i.e.

$$C_N = \frac{(\mathbf{G}^N)_{1,5}}{N l_{rep}^2} \tag{15}$$

where $(\mathbf{G}^N)_{1,5}$ is the element at the first row and fifth column of the 5 × 5 matrix $\mathbf{G}^N$, and

$$l_{rep}^2 = \sum_{i=1}^{10} l_i^2 \tag{16}$$

The calculation with the numbers provided in Tables 1−3 leads to a limiting characteristic ratio of 5.0 as $N \to \infty$. This number is smaller than the estimate of $C_\infty = 6.4$ for a PI-2 single chain in vacuum at 300 K,[28] suggesting that the mean-square dimensions of PI-2 are reduced by about 20% due to packing in a bulk amorphous structure.

The most substantial change from an isolated chain to the bulk in Tables 1−3 lies in ϕ_6 and ϕ_9, for which the average cosines are changed from −0.867 in the isolated chain to −0.427 in the bulk. If we keep all parameters the same as for the single chain except for substituting the bulk value of the average cosines of ϕ_6 and ϕ_9 (−0.427) for their single-chain value (−0.867) in the calculation of the characteristic ratio, we obtain a value of $C_\infty = 5.17$. From this observation it is evident that the reduction in C_∞ arises almost entirely from the appearance of the new rotational isomeric states near *gauche* and *gauche'* at bonds 6 and 9 in the repeat unit.

5. Cohesive Energy and Hildebrand Solubility Parameter. The cohesive energy, E_{coh}, of a polymer in the bulk is the decrease in energy as different polymer chains are brought together from infinity. The cohesive energy in our case can be calculated by the difference in the potential energies between the parent chain in the bulk and the parent chain as a single chain, i.e.

$$E_{coh} = E_{parent} - E_{bulk} \tag{17}$$

The Hildebrand solubility parameter, δ, is defined in terms of the cohesive energy density, E_{coh}/V, where V is the volume of the amorphous cell,

$$\delta = (E_{coh}/V)^{1/2} \tag{18}$$

For the cells with $x = 13$ and the cells with $x = 14$, we obtained the cohesive energies and Hildebrand solubility parameters as the following:

$$E_{coh,13} = 728 \pm 13 \text{ kcal/mol (per 13 repeat units)} \tag{19}$$

$$E_{coh,14} = 794 \pm 29 \text{ kcal/mol (per 14 repeat units)} \tag{20}$$

$$\delta_{13} = 11.3 \pm 0.1 \text{ (kcal/cm}^3\text{)}^{1/2} \tag{21}$$

$$\delta_{14} = 11.4 \pm 0.1 \text{ (kcal/cm}^3\text{)}^{1/2} \tag{22}$$

where the last figure in each equation is the standard deviation. The small magnitude of the standard deviations indicates that the simulation has a good degree of confidence. The calculated Hildebrand solubility parameter, ~11.3 (kcal/cm^3)$^{1/2}$, is somewhat larger than that calculated for the amorphous polysulfone without partial charges, 8.29 (kcal/cm^3)$^{1/2}$,[8] and what was calculated for the amorphous polycarbonate with partial charges, 9.6 (kcal/cm^3)$^{1/2}$.[3]

Conclusions

We have studied some bulk properties of amorphous PI-2 with atomistic modeling. We have analyzed the atomic radial distribution functions and the correlations between the phenyl rings in the structures to show that no long-range order exists in the structures. Some order of the phenyl rings does exist due to the van der Waals interactions, but only in the very short range of 3.5−4.5 Å. The packing of a PI-2 chain in an amorphous structure changes the conformational statistics of the chain and reduces the chain dimension relative to a PI-2 single chain at 300 K. The reduction in the chain dimension is evidenced by a decrease of the characteristic ratio relative to the single chain. It is further shown that the appearance of the two new rotational

isomeric states at bonds 6 and 9 in the repeat unit is almost entirely responsible for such a reduction. The Hildebrand solubility parameter of amorphous PI-2 is calculated from the cohesive energy density of the structures. The consistency in the numbers obtained from the set of amorphous cells with 13 PI-2 repeat units and the set with 14 repeat units and the small magnitude of the standard deviations both indicate that the sizes of the amorphous cells in the simulation are adequate and estimates obtained from this method should be reliable.

Acknowledgment. This research was supported by the NSF-EPIC Center for the Molecular and Microstructure of Composites.

References and Notes

(1) Rigby, D.; Roe, R. J. *J. Chem. Phys.* **1987**, *87*, 7285.
(2) Theodorou, D. N.; Suter, U. W. *Macromolecules* **1985**, *18*, 1467.
(3) Hutnik, M.; Gentile, F. T.; Ludovice, P. J.; Suter, U. W.; Argon, A. S. *Macromolecules* **1991**, *24*, 5962.
(4) Lee, K. J.; Mattice, W. L. *Comput. Polym. Sci.* **1992**, *2*, 55.
(5) Li, Y.; Mattice, W. L. *Macromolecules* **1992**, *25*, 4942.
(6) Kim, E. G.; Misra, S.; Mattice, W. L. *Macromolecules* **1993**, *26*, 3424.
(7) Rigby, D.; Roe, R. J. *Chem. Phys.* **1988**, *89*, 5280.
(8) Fan, C. F.; Hsu, S. L. *Macromolecules* **1991**, *24*, 6244.
(9) Smith, G. D.; Jaffe, R. L.; Yoon, D. *Macromolecules* **1993**, *26*, 298.
(10) Rigby, D.; Roe, R. J. *Macromolecules* **1990**, *23*, 5312.
(11) Arizzi, S.; Mott, P. H.; Suter, U. W. *J. Polym. Sci., Polym. Phys. Ed.* **1992**, *30*, 415.
(12) Greenfield, M. L.; Theodorou, D. N. *Macromolecules* **1993**, *26*, 5461.
(13) Misra, S.; Mattice, W. L. *Macromolecules* **1993**, *26*, 7274.
(14) Trohalaki, S.; Kloczkowski, A.; Mark, J. E.; Roe, R. J.; Rigby, D. *Comput. Polym. Sci.* **1992**, *2*, 147.
(15) Pant, P. V. K.; Boyd, R. H. *Macromolecules* **1993**, *26*, 679.
(16) Müller-Plathe, F. *J. Chem. Phys.* **1992**, *96*, 3200.
(17) Gusev, A. A.; Arizzi, S.; Suter, U. W.; Moll, D. *J. Chem. Phys.* **1993**, *99*, 2221.
(18) Gusev, A. A.; Suter, U. W. *J. Chem. Phys.* **1993**, *99*, 2228.
(19) Rigby, D.; Roe, R. J. *Macromolecules* **1989**, *22*, 2259.
(20) Takeuchi, H.; Roe, R. J. *J. Chem. Phys.* **1991**, *94*, 7446.
(21) Takeuchi, H.; Roe, R. J. *J. Chem. Phys.* **1991**, *94*, 7458.
(22) Ludovice, P. J.; Suter, U. W. In *Computational Modeling of Polymers*; Bicerano, J., Ed.; Marcel Dekker: New York, 1992; p 401.
(23) Hutnik, M.; Argon, A. S.; Suter, U. W. *Macromolecules* **1993**, *26*, 1097.
(24) Hutnik, M.; Argon, A. S.; Suter, U. W. *Macromolecules* **1991**, *24*, 5956.
(25) Hutnik, M.; Argon, A. S.; Suter, U. W. *Macromolecules* **1991**, *24*, 5970.
(26) Harris, F. W.; Lien, H. S.; Zhang, Y.; Tso, C. C.; Gabori, P. A.; Cheng, S. Z. D. *Polym. Prepr. (Am. Chem. Soc., Div. Polym. Chem.)* **1991**, *32* (2), 201.
(27) Cheng, S. Z. D.; Mittleman, M. L.; Janimak, J. J.; Shen, D.; Chalmers, T. M.; Lien, H.-S.; Tso, C. C.; Gabori, P. A.; Harris, F. W. *Polym. Int.* **1992**, *29*, 201.
(28) Zhang, R.; Mattice, W. L. *Macromolecules* **1993**, *26*, 6100.
(29) Mayo, S. L.; Olafson, B. D.; Goddard, W. A. *J. Phys. Chem.* **1990**, *94*, 8897.
(30) See: *Polymer Handbook*, 2nd ed.; Brandrup, J., Immergut, E. H., Eds.; Wiley-Interscience: New York, 1975; p VIII-7.
(31) Rappé, A. K.; Goddard, W. A., III *J. Phys. Chem.* **1991**, *95*, 3358.
(32) Rapold, R. F. Ph.D. Thesis, ETH, 1990; pp 79–88.
(33) Flory, P. J. *Statistical Mechanics of Chain Molecules*; Wiley: New York, 1969.
(34) Mattice, W. L.; Suter, U. W. *Conformational Theory of Macromolecules, The Rotational Isomeric State Model in Macromolecular Systems*; Wiley: New York, 1994.
(35) Flory, P. J. *Macromolecules* **1974**, *7*, 381.

MA946177T